

# Remote Monitoring of Resin Transfer Molding Processes by Distributed Dielectric Sensors

MICHAEL C. HEGG,<sup>1</sup> ANIL OGALE,<sup>2</sup> ANN MESCHER,<sup>2</sup>  
ALEXANDER V. MAMISHEV<sup>1,\*</sup> AND BOB MINAIE<sup>3</sup>

<sup>1</sup>*Department of Electrical Engineering, University of Washington, 253 EE/CSE Bldg  
Box 352500, Seattle, WA 98195-2500, USA*

<sup>2</sup>*Department of Mechanical Engineering, University of Washington, 324 ME Bldg  
Seattle, WA 98195-2600, USA*

<sup>3</sup>*Department of Mechanical Engineering, Wichita State University  
Wichita, KS 67260, USA*

(Received December, 2003)  
(Accepted November 8, 2004)

**ABSTRACT:** Feed-forward adaptive control of resin transfer molding (RTM) processes is crucial for producing a high yield of usable parts for industrial applications. The enabling technique for this process is non-invasive monitoring of the fill-front position and the degree of cure of the resin as it is injected into the mold. Successful implementation of a sensing system capable of meeting these criteria will result in a high yield of composite parts that can be used for the next generation of aircraft. This article articulates the possibility of a hybrid sensing system for multiparameter monitoring during RTM processes. It addresses the fundamental engineering trade-offs between penetration depth and signal strength, discussing how to account for fringing electric field (FEF) effects present in the system. FEF effects hinder the measurement accuracy of the sensor system. This article describes how these effects are addressed using a mapping algorithm that is developed using numerical simulations of the experimental setup. The experimental setup utilizes a rectangular RTM tool and a water-glycerin mixture which simulates mechanical properties of epoxy resins, prior to cure. Modeling of the FEF effects helps to achieve high measurement accuracy of the fill front location.

**KEY WORDS:** dielectric sensors, resin transfer molding, composite material manufacturing, adaptive control.

---

\*Author to whom correspondence should be addressed. E-mail: mamishev@ee.washington.edu

## INTRODUCTION

**R**ESIN TRANSFER MOLDING is a widely used composite material manufacturing process that produces high-strength and lightweight parts for various industrial applications. Dry spot formation is a phenomenon that can seriously jeopardize the mechanical integrity of the part [1,2]. Dry spots occur when the resin cannot fully wet the preform. Dry spot formation is strongly dependent on such processing parameters as temperature, viscosity, pressure, and fill-front location. In order to manufacture defect-free parts with consistent material properties, it is important to monitor and control these parameters throughout the entire volume of the mold. The measured physical variables can be used as inputs for the adaptive process control algorithm designed to optimize the manufacturing process [3,4]. The fill-front position has been identified as a crucial parameter in determining last-point-to-fill (LPF) and dry spot formation [5]. Previous attempts to regulate fill-front location have shown limited controllability [6–8].

Many techniques have been used to monitor the resin transfer molding process, including fiber optical sensing [9–11], ultrasound sensing [12,13], fluorescence [14], calorimetry [15], and DC resistance measurements [5,16–18]. These techniques are similar in that they all require either embedded sensing elements or partial contact with the parts. DC resistance measurement arrays, such as SMARTWEAVE, provide the ability to monitor the fill-front position and the degree of cure simultaneously. However, this technique relies on point sensing, where the resolution of important parameters, like the fill-front location, is limited by the number of sensor pixels the system can handle. A system capable of continuously sensing fill-front progression can more accurately determine the velocity and position of the fill-front.

A promising candidate technology to base an adaptive control system on is AC dielectrometry. This technique is capable of sensing fill-front location, curing, temperature, and viscosity simultaneously [19,20]. FDEMS is a commercially available AC dielectrometry system that relies on point sensing and requires direct contact and embedded parts [21–24]. It has been shown in [25,26] that AC dielectric sensors are capable of accurately measuring fill-front position and degree of cure. In [26], a linear dependence of the admittance signal on the fill-front position is shown. This type of sensor relies on fringing electric fields and allows continuous sensing of fill-front progression in one dimension. The system designed by Rooney et al. [25] is a three-channel sensing system capable of converting capacitance to voltage and correlating this to flow-front position. This system is limited to sensing fill-front location, and does not provide the ability to measure resin properties. The system discussed in this article is designed to perform spectroscopy measurements (i.e., measurements at multiple frequencies) and combine point sensing with continuous sensing.

Dielectric spectroscopy of material properties was deeply investigated by Von Hippel in the 1940s [27]. More advanced techniques based on the measurement of the dielectric properties of the polymer composites, including interdigital dielectrometry, were developed by Matis in the 1960s [28]. Microdielectrometry as a means of measuring dielectric properties in polymers was developed and used by Senturia's group in the early 1980s [29–31], and subsequently by other groups during the last ten years [32–35]. The recent trend has been to integrate dielectric spectroscopy into a self-contained system capable of measuring multiple parameters of interest for material manufacturing processes.

In the case of this study, viscosity, temperature, and degree of cure must be inferred from the measurements of capacitance and conductance between the sensor array electrodes. This project is focused on the design and implementation of a sensor system that can measure the desired parameters of interest with the required accuracy, spatial resolution, and speed. In order to measure viscosity, temperature, and degree of cure in 3D, a sensor that can perform spectroscopy measurements at many different points along the mold should be designed. Although spectroscopy measurements are inherently discrete in space and time, a large number of pixel elements will make these measurements more useful. Conversely, the measurement of the fill-front does not require spectroscopy and should be sensed continuously for the most accurate results. Thus, a sensing system capable of measuring multiple parameters of interest should have multiple sensing elements. The first type of element should be designed to measure the fill-front location of a liquid material as it flows through the mold. The second type of element should be designed to perform dielectric spectroscopy measurements at discrete points in space. Both types of elements can be duplicated several times to compose a larger array of pixels. Figure 1 shows a conceptual illustration of how the flow-front and spectroscopy pixels can be integrated into a hybrid sensor array. Figure 1 is designed to give the reader an idea of the global view that this article is driving towards, and is not meant to illustrate an existing sensing system.

This article describes the design and testing of the fill-front element of a multipixel sensor system. This is an important first step in the realization of a hybrid sensing system that can be used for adaptive control in RTM. The design and testing of the spectroscopy sensor elements shown in Figure 1 will be detailed in a later publication. This sensor system will have continuous dielectric sensing capabilities for remote and *in situ*

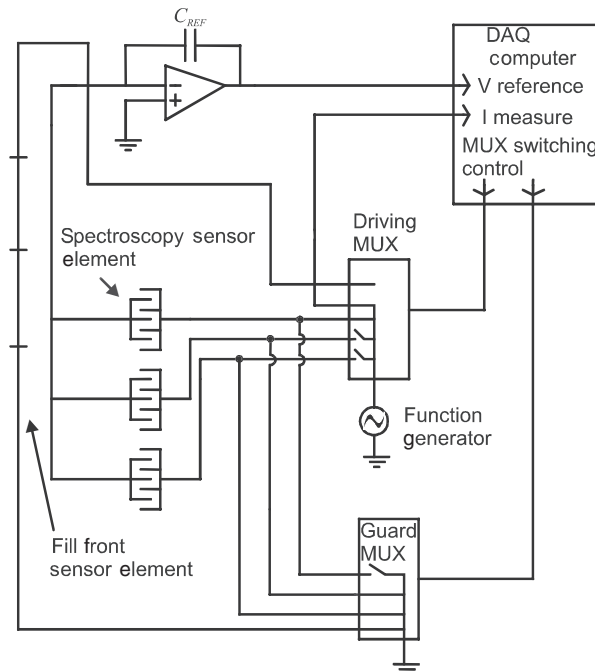


**Figure 1.** Conceptual layout of a hybrid sensor that shows fill-front and spectroscopy sensing elements connected to multiplexing circuitry.

monitoring of the fill-front position, viscosity, temperature, and the degree of cure during resin transfer molding. These sensors will rely on continuous and simultaneous measurements of transmittance matrix entries over a wide range of frequencies. The prototype sensor system described in this article has been integrated with a resin transfer molding apparatus, and is composed of three sensors, a three-channel circuit capable of measuring gain and phase, a function generator, DC power supply, and data acquisition software. An AC sinusoidal signal is supplied by the function generator to the bottom plate of the mold (aluminum). Electric field is generated between the bottom plate and the sensors resting on top of the upper polycarbonate (Lexan) plate of the mold. The sensors react to the changes in capacitance and conductance due to resin injection and progression through the mold. Numerical simulations of the sensors allow for the calculation of the fill-front position along the mold based on the measured signal strength.

The following section discusses the experimental system. The next section after that details the experimental results obtained with several types of FEF sensors. Finally, conclusions are presented.

## EXPERIMENTAL SYSTEM

An RTM laboratory setup, including the mold, resin flow system, and digital camera for flow verification, was used to simulate the industrial resin transfer molding process. To monitor important processing parameters, a sensor system with three channels and continuous sensing capability was designed and integrated into the resin transfer molding setup. A three-channel buffer circuit was custom-built for this project to interface with the sensor system and output the measurements in real time using LabView software. This section discusses the elements of the RTM laboratory setup. Mold and materials are discussed, followed by the discussion of the sensor design and fabrication. Finally, the data acquisition circuit and software are presented.

### RTM Laboratory Setup

Figure 2 shows the experimental system consisting of a resin transfer mold, a fluid delivery system, and sensors. The mold is rectangular with a transparent upper plate for visualization of the fill-front. The working fluid is delivered to the mold using a pressurized reservoir. A video camera is mounted above the mold in a steel frame. Dielectric sensors are used to monitor the fill-front. The preform used in this study is an open-celled polyurethane foam (MA70) with a uniform permeability throughout the material. The permeability of the medium is determined from Darcy's law using measured fill-front velocities and pressure gradients. The foam has a solid fraction of 3.8%. The fill-front velocity is calculated using the change in fill-front position over a known interval of time. The pressure gradient is obtained from pressure measurements within the mold cavity using a Wilkerson USG pressure gauge with a scale of 0–30 Hg. A mixture of 80% glycerin and 20% water is used as the working fluid. The viscosity of glycerin solution is similar to that of the resins used and it also does not wick into the foam. This allows for easy cleaning and fast sequencing of the experiments. For filling experiments, the dielectric properties of the working fluid need not be similar to that of industrial resins as long as the viscosities are similar and the fluids flow in the same manner. A rectangular aluminum

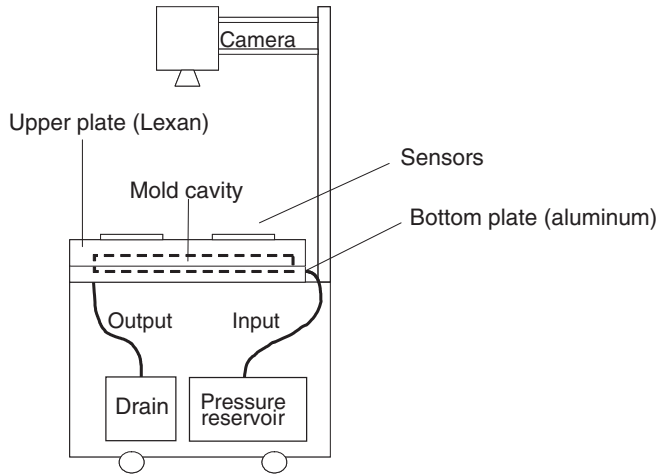


**Figure 2.** RTM mold and video camera that allows for independent measurements of fill-front position.

mold  $350 \times 250 \times 10 \text{ mm}^3$  with one inlet port and one outlet port is used as the mold cavity. A 38-mm thick Lexan plate serves as the upper assembly of the mold. A digital video camera is mounted 1 m from the top of the mold to record the fill-front position independently. The mold is assembled by clamping the two aluminum plates together with bolts. Glycerin–water solution is delivered to the mold from the pressure pot using flexible tubing. The preform used is 19 mm shorter than the mold cavity to allow for pressure equalization on the leading edge to ensure a one-dimensional fill-front. Multiple trials were performed to ensure repeatability of the system. Experiments were conducted for varying reservoir pressures ranging from 69 kPa (10 psi) to 114 kPa (16.5 psi), at room temperature.

Figure 3 shows the geometrical distribution of sensors on the top of the Lexan plate. This geometry allows for comprehensive and continuous sensing of the fill-front. The sensors are aligned parallel to the expected direction of the glycerin flow-front movement. BNC cabling is used to connect the function generator to the top plate of the aluminum mold. For all experiments reported here, the function generator supplied a constant 6 V sinusoidal signal at 1 kHz driving frequency. An electric field is generated between the sensors and the mold with the applied signal. The progression of the fill-front is detected by continuously sensing a change in the complex gain, i.e., the ratio of the output and input voltages for each sensor pixel. Changes in capacitance and conductance are then inferred from changes in complex gain using a simple impedance divider circuit. Figure 4 shows the general schematic of the experimental system.

## Sensors

### THEORY

It is well known that impedance cells can be used to sense the properties of dielectric materials [36,37]. In the simplest case, two parallel electrodes with equal but opposite surface charge densities  $\sigma_s$  have a potential difference

$$V = \phi_1 - \phi_2 \quad (1)$$

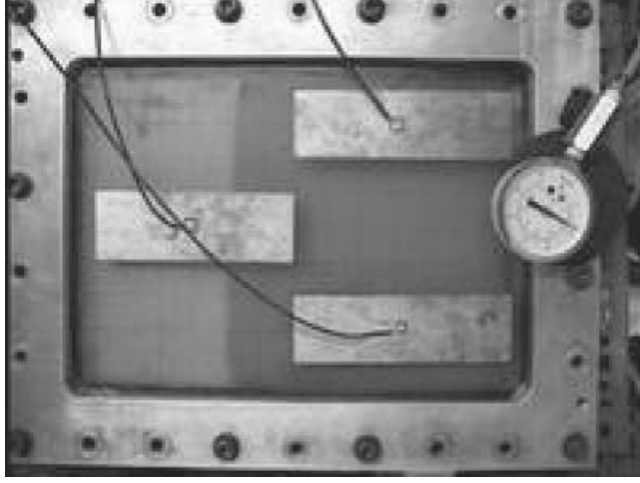


**Figure 3.** Experimental setup with distributed dielectric sensors. Fill-front position is inferred as the water-glycerin solution passes under the sensor.

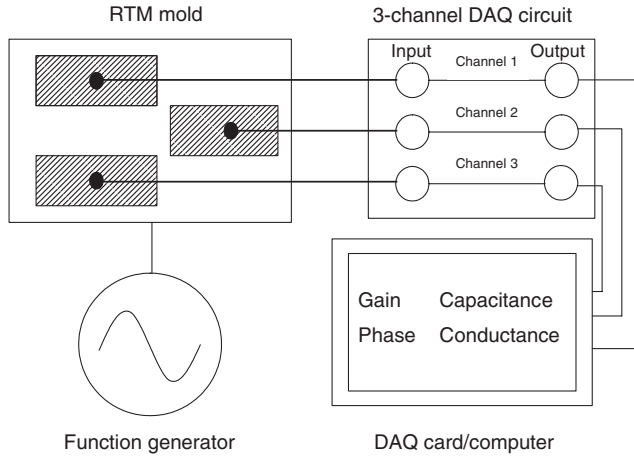


**Figure 4.** General schematic of the experimental system with data acquisition.

where  $\phi_1$  and  $\phi_2$  represent electric potential on each electrode. Since the potential difference is equal to the work required to move charge from one plate to the other,

$$V = \mathbf{E}d \quad (2)$$

where  $d$  is the distance between the electrodes. From Gauss' law, the electric field  $\mathbf{E}$  between the electrodes is

$$\mathbf{E} = \frac{\sigma_s}{\epsilon} \quad (3)$$

It follows that

$$V = \frac{\sigma_s}{\epsilon} d = \frac{d}{\epsilon A} Q \tag{4}$$

The total charge,  $Q$ , on both electrodes is proportional to the potential difference between the electrodes. The constant of proportionality is the capacitance and is given by

$$C = \frac{\epsilon A}{d} \tag{5}$$

and the conductance is given by

$$G = \frac{\sigma A}{d} \tag{6}$$

where  $\sigma$  is the conductivity of the material.

When a dielectric material is passed between the plates of the mold, the capacitance  $C$  and the conductance  $G$  change. Guard electrodes are usually included in the parallel-plate configuration to ensure a uniform electric field within the sensing area. Figure 5 shows the distribution of the electric field lines in a guarded parallel-plate sensor. The figure shows that the electric field lines are attracted to regions of greater permittivity, and thus how fringing fields can exist even in guarded parallel-plate sensors. A video camera is used to make independent measurements of the fill-front position to test the accuracy of the sensor system. For the experiments reported in this article, a three-element dielectric sensor array is used to detect the fill-front position of glycerin–water solution as it is injected into a mold.

A 6-V amplitude sinusoidal input signal is applied to the bottom plate of the mold. Each sensor outputs to a channel on an impedance divider circuit. The complex voltage signal

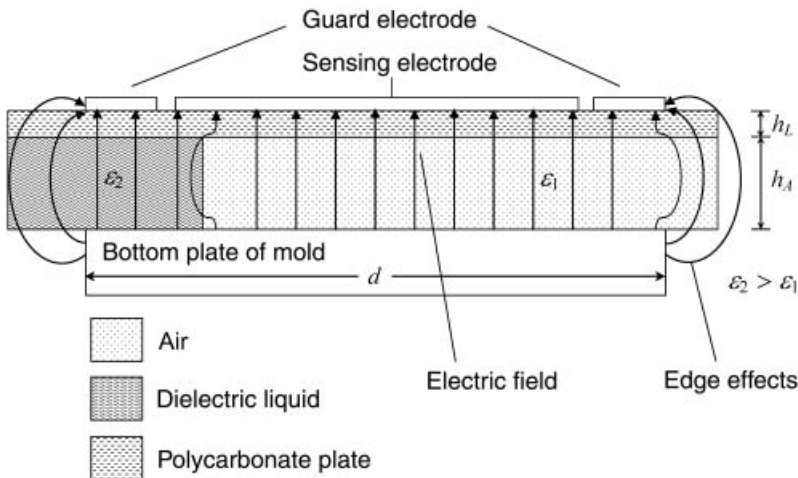


**Figure 5.** Distribution of the electric field of the sensor including the edge effects. Fluid flows into the mold cavity, and the position is inferred from changes in capacitance.

is fed into a PC via a DAQ card operating at 96 kS/s. Data acquisition software was written in LabView to convert the measured gain and phase to capacitance and conductance, and display these values in real time.

### **Design Constraints**

Figure 5 shows how the composition of the material can affect the uniformity of the electric field in the parallel-plate sensor. Besides material composition, the uniformity of the electric field is strongly dependent on the geometry of the sensor. For a parallel-plate configuration, the parameters of the setup that affect the uniformity of the electric field are the distance between the electrodes, the composition of the material, and the degree to which the electrodes are parallel to each other. If the material between the electrodes is nonhomogeneous or the distance between the electrodes varies considerably over the sensing area, the electric field can be non uniform and the capacitance measured is then based on an average value of the dielectric permittivity over the sensing area. As long as the electrodes are parallel, the material homogeneous, and the distance between the electrodes relatively small, the electric field will be uniform.

It may be possible to quantify the effect of the electric field for a given part geometry. A more practical solution, however, would be to utilize a fringing electric field (FEF) setup, where the electric field fringes into the part and only one-sided access is needed. This would allow for point sensing within the part and allow for complex part geometries where parallel-plate setups become impractical.

The shape of the sensor can be designed to accommodate different mold geometries and for optimal adaptive control needs. Sensing area is the most important design criterion for parallel-plate sensors, and therefore long strips are commonly used. For FEF sensors, the spacing between the electrodes determines the penetration depth. Longer and thinner sensor geometries will not accommodate as many electrodes as a wider design. For our purposes, however, one fringing electric field is adequate and therefore a longer and thinner sensor is realizable.

As demonstrated in [38], FEF sensors can be bent (e.g., wrapped around objects with complex geometries) with no measurable effect on their performance. This is of importance in composite material manufacturing processes, where the mold geometry is complex. In addition, it may be possible to line the walls of the mold with complex sensor shapes in order to achieve a more uniform sensing of the part. Parallel-plate sensors can be designed to be thin, transparent, and flexible. The sensors can be laminated with a protective coating to ensure mechanical integrity under extreme temperatures and prevent damage from spills.

### **Fabrication**

Transparent dielectric sensor heads were fabricated using standard photolithography techniques: indium tin oxide (ITO) was evenly sputtered onto one side of a thin polyester film, a mask of the sensor electrode pattern was placed over the film, and exposed to UV light. The sensor pattern was etched into the ITO using bleach as an etching agent. Optically transparent glue was then used to attach an unetched sheet of ITO film to the backside of the newly etched sheet. This blank sheet of ITO serves as the backplane for



**Figure 6.** Flexible, transparent sensor head.

the sensor head. Finally, both sides of the sensor head were cold-laminated using commercially available lamination sheets, which serve as a protective coating against scratches. Coaxial cables are attached to the sensor head via zero-insertion-force (ZIF) connectors. The transparency of the sensor head allows for complete visual confirmation of flow-front position and offers the possibility of enhancing the system with an infrared sensor. Figure 6 shows the complete ITO sensor head.

### **Data Acquisition and Sensor Interface**

The data acquisition and sensor interface consists of a custom-designed buffer circuit that interfaces the sensor head with a computer, and software that displays sensor measurements in real time. For every operating frequency, when a dielectric material is placed between two parallel conducting electrodes, the resultant circuit can be modeled as an RC parallel combination. For sensor impedance measurements, the custom designed three-channel circuit utilizes a floating-voltage measurement technique. Figure 7 shows a single measurement channel, where the voltage divider is formed by the sensor and the reference impedance. The voltage is sensed by an ultra-high input impedance op-amp in a voltage follower configuration. The reference impedance value is set close to the value of the expected measurement impedance. When the material under test is only weakly conductive, the lumped circuit approximation can be simplified to a single capacitor. The reference capacitance value used in these experiments is 7 pF for each of the three channels.

The coaxial cable connecting a sensor to the measurement circuit is 1.5 m long. To eliminate the effect of capacitance between the inner and the outer conductor in the cable, the output of the voltage follower is fed back to the cable's shielding conductor. The technique ensures that there is no potential difference between the inner conductor carrying the sense signal and the shielding conductor around it. The shield potential is also used to keep the guard electrode at the same potential as the sensing electrode.

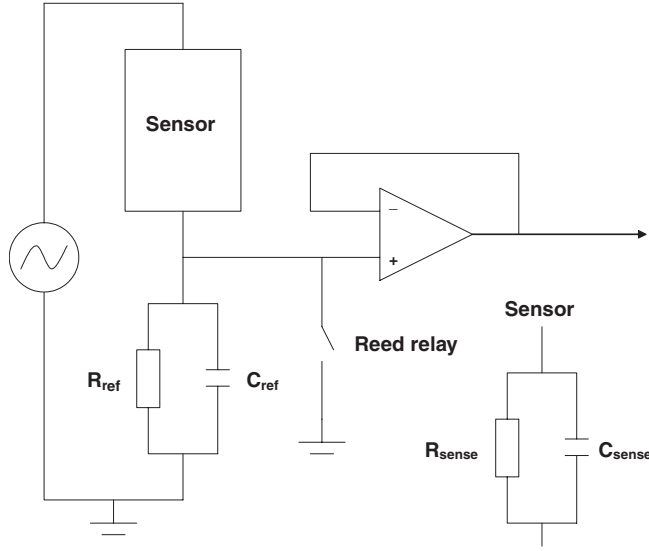


**Figure 7.** Circuit schematic for a single channel.

For the specified sensor geometry, the capacitances in the voltage divider are usually very small. The leakage current from the op-amp input causes a static charge to accumulate on the senso electrodes, as well as on the reference capacitor. To discharge both capacitances, a reed relay is connected between the middle of the voltage divider and the ground terminal. The switch is automatically closed for a short period of time before each measurement.

The outputs of the three-channel circuit and the function generator signal are connected to a NI-DAQ 6035E data acquisition card operating at 96 kS/s. The card simultaneously samples all four voltage signals. In addition, it provides the digital signal for controlling the discharge relays. It should be noted that the input impedance of the NI card when connected to the output of the op-amp can greatly decrease the phase margin of the circuit, causing high-frequency instability. To prevent possible oscillatory behavior, a 1 k $\Omega$  resistance can be added between each of the circuit's outputs and the positive power supply rail.

Software was written in LabView to acquire a complex voltage signal from each channel on the circuit and reduce this signal to its gain and phase components. The conductance and capacitance can be inferred from (7) and (8), respectively, where  $V$  is the gain,  $\theta$  is the phase,  $\omega$  is the angular frequency,  $C_r$  is the reference capacitance, and  $G_r$  is the reference conductance.

$$G_{\text{sense}} = -\frac{V \cdot (\sin(\theta) \cdot \omega \cdot C_r - \cos(\theta) \cdot G_r + V \cdot G_r)}{V^2 - 2 \cdot V \cdot \cos(\theta) + 1} \quad (7)$$

$$C_{\text{sense}} = -\frac{V \cdot (-\omega \cdot C_r \cdot \cos(\theta) + \omega \cdot V \cdot C_r - \sin(\theta) \cdot G_r)}{\omega \cdot (V^2 - 2 \cdot V \cdot \cos(\theta) + 1)} \quad (8)$$

## RESULTS AND DISCUSSION

This section first discusses numerical results for the predicted fill-front position and compares these results to the experimentally observed fill-front position. Developing analytical equations that can accurately predict the fill-front position is an important step in being able to implement adaptive control in RTM. Numerical simulations of the sensor will then be discussed, followed by the experimental results obtained with the RTM setup using water–glycerin filler and by results obtained with the VARTM setup using polymer resins.

### Predicted Fill-front Position

The average fluid velocity  $\bar{V}$  through the porous preform is

$$\bar{V} = \frac{Q_{\text{mold}}}{A_{\text{frac}}} \quad (9)$$

where  $Q_{\text{mold}}$  is the volumetric flow rate in the mold and  $A_{\text{frac}}$  is the cross-sectional area of the mold perpendicular to the direction of the flow and not occupied by the porous medium. From Darcy's law, the flow from the leading edge of the porous medium to the fill-front is described by

$$\bar{V} = -\frac{k}{\mu} \frac{\partial P}{\partial x} \quad (10)$$

where  $\bar{V}$  is the average velocity of the fluid,  $k$  is the permeability of the porous medium,  $\mu$  is the viscosity of the fluid and  $(\partial P/\partial x)$  is the pressure gradient in the  $x$  direction. The pressure change for a one-dimensional flow through an isotropic porous medium is linear. Therefore the average velocity can be written as

$$\bar{V} = \frac{k}{\mu} \frac{P_{\text{in}} - P_{\text{fill-front}}}{x} \quad (11)$$

where  $x$  is the distance from the leading edge of the porous medium to the fill-front and  $P_{\text{in}}$  is a function of  $x$ . Expressing the pressures as gauge pressures, (9) and (11) can be combined to give

$$\bar{V} = \frac{dx}{dt} = \frac{k}{\mu} \frac{P_{\text{in}}}{x} \quad (12)$$

since  $P_{\text{fill-front}}$  is the atmospheric pressure. A complete derivation of  $P_{\text{in}}$  is given in [39]. The result is stated here:

$$P_{\text{in}} = \frac{A + B \pm \sqrt{(A + B)^2 - 32CD^4[P_{\text{res}} - \rho g(h_0 + (A_{\text{fr}}/A_{\text{re}})x)]}}{(16C/\pi)} \quad (13)$$

where

$$A = 128l_{\text{eq}} \frac{kA_{\text{fr}}}{x} \quad (14)$$

$$B = \pi D^4 \quad (15)$$

$$C = \rho \left( \frac{kA_{\text{fr}}}{\mu x} \right)^2 \quad (16)$$

$x$  is the flow-front location,  $P_{\text{in}}$  is the inlet pressure recorded,  $l_{\text{eq}}$  is the equivalent length of tubing,  $k$  is the permeability of porous medium,  $A_{\text{fr}}$  is the cross sectional area of the mold perpendicular to the direction of the fluid flow not occupied by the porous material,  $A_{\text{re}}$  is the cross sectional area of the reservoir,  $\mu$  is the viscosity of the fluid,  $D$  is the inside diameter of the tube,  $P_{\text{res}}$  is the pressure in the pressure pot,  $h_0$  is the initial height difference between the fluid level in the pot and the inlet port when the fill-front is at the leading edge of porous medium, and  $\rho$  is the density of the fluid. The values used in the numerical simulation are  $l_{\text{eq}} = 0.66$  m,  $A_{\text{fr}} = 0.00309$  m<sup>2</sup>,  $D = 0.00432$  m,  $\rho = 1220$  kg/m<sup>3</sup>,  $h_0 = 0.4$  m,  $A_{\text{re}} = 0.0415$  m<sup>2</sup>,  $\mu = 0.089$  Ns/m<sup>2</sup>, and  $k = 2.51 \times 10^{-9}$  m<sup>2</sup>. The viscosity and density values of the water-glycerin solution were taken from the manufacturer's specification sheet.

Equation (12) can be rearranged as follows to give the fill-front position as a function of time

$$\int_0^t \frac{k}{\mu} dt = \int_0^x \frac{x'}{P_{\text{in}}} dx' \quad (17)$$

$$\frac{k}{\mu} t = \int_0^x \frac{x'}{P_{\text{in}}} dx' \quad (18)$$

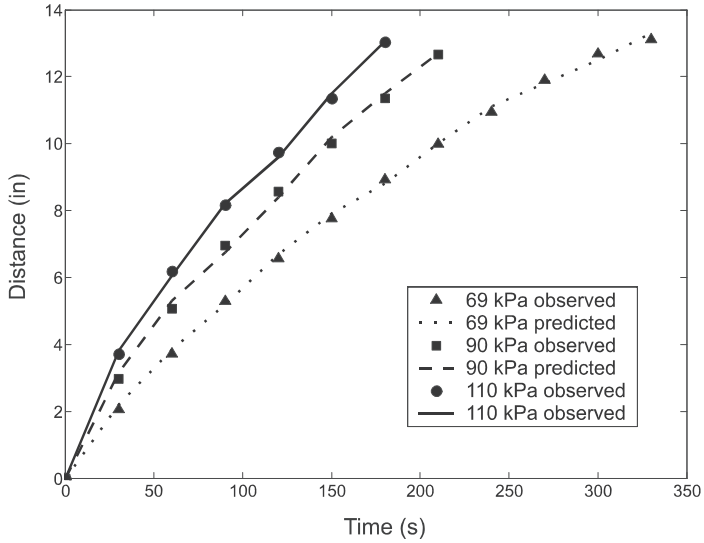
Equation (18) expresses the fill-front position at any time as a function of the reservoir pressure alone. It is numerically solved for  $x$  after substituting for  $P_{\text{in}}$  from (13).

Figure 8 shows comparisons between experimental data obtained visually and predicted data for varying reservoir pressures. As the pressure was increased, a corresponding fall in the fill time was observed. It was also noted that there was a slight deviation of predicted values from the experimental results, which could be attributed mostly to a rounding error in the inlet pressure readings.

The good agreement between visually recorded flow-front position and theoretically predicted position suggests that the system is sufficient for simulating industrial resin transfer molding processes. It follows that a sensor technique capable of monitoring flow-front position on this system will also measure the position accurately on an industrial setup.

### Predicted Sensor Performance

The numerical simulations were performed using Maxwell software by Ansoft Corp. Each transparent sensor was modeled as a cross section of infinite depth on a per-meter length basis. A parametric simulation of each sensor was run in order to find the predicted



**Figure 8.** Comparison between experimental (visual) and predicted data for varying reservoir pressures (69, 90, 110 kPa).

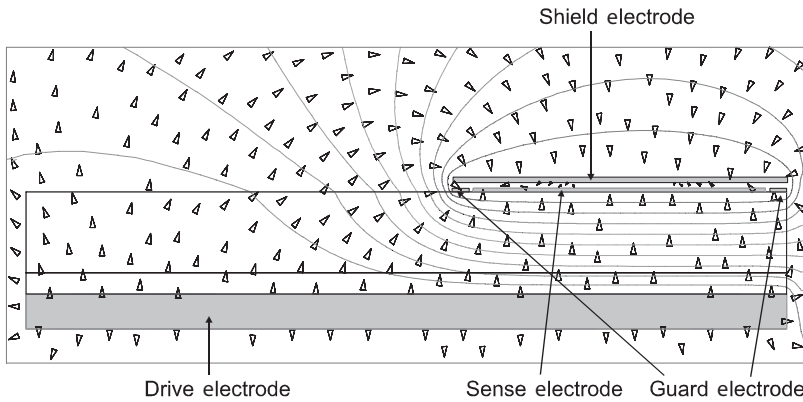


**Figure 9.** Equipotential lines and distribution of the electric field in and around the dielectric cell. The size of the arrows is logarithmically proportional to the intensity of the electric field.

capacitance as a function of flow-position along the mold. Figure 9 shows the distribution of equipotential lines and electric field in and around the dielectric cell. Figure 9 also shows the uniformity of the field between the sensing and driving electrodes, whereas the field begins to fringe between the guard and the drive electrodes. Figure 10 shows the results of the numerical simulation for a single sensor.

The numerical simulations are used to produce an accurate transfer function between the measured capacitance and conductance values and the position of the fill-front inside the mold. In the absence of fringing field effects, the sensors would record fill-front progression only when the liquid is directly between the sensing and driven electrodes of the parallel-plate setup. Since the exact position of the sensors on the mold is known a priori, a measurable change in sensor signal directly corresponds to the position

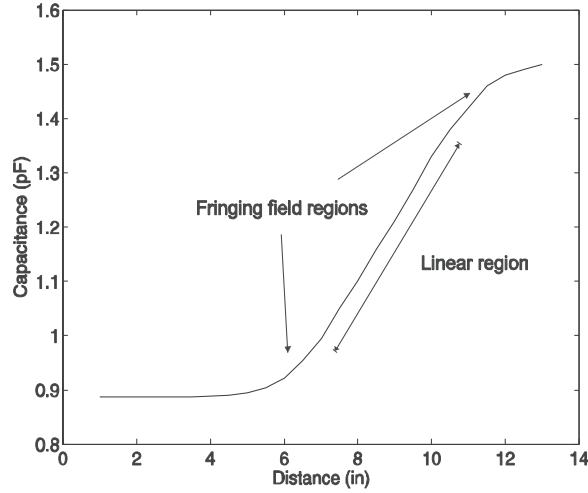


**Figure 10.** Numerical results for a single sensor. The geometry and position of the sensor on the mold determines the characteristic curve.

of the fill-front. Fringing field effects, however, cause the sensor to measure fill-front progression before the liquid is directly underneath the sensor, thus preventing a direct calculation of the fill-front position from the measured capacitance and conductance. These effects can be seen in the early and late stages of the numerical data shown in Figure 10.

It is important to compare the numerical results to theoretically predicted values for a guarded parallel-plate capacitor in order to ensure the accuracy of the simulation. The analytical expression for the capacitance of the heterogeneous material inside the mold can be calculated using a lumped circuit approximation of the layered medium. The capacitance contributed by the dielectric permittivity of the Lexan plate and air can be represented by a series combination of capacitors. When the mold fills, the air is replaced with water–glycerin solution and the capacitor previously representing the air now represents the water–glycerin solution. The analytical expression for the capacitance is

$$C = \varepsilon_0 \cdot A \cdot \left[ \frac{1}{(d_1/\varepsilon_1) + (d_2/\varepsilon_2)} \right] \quad (19)$$

where  $A$  is the area of the sensing electrode,  $d_1$  is the thickness of the Lexan plate,  $d_2$  is the air gap thickness, and  $\varepsilon_1$  and  $\varepsilon_2$  are the dielectric permittivities of Lexan and air, respectively. For this study  $\varepsilon_1 \approx 3.1$  and  $\varepsilon_2 \approx 1$ . The presence of preform typically increases  $\varepsilon_2$  by a factor of 1.1 to 1.5. The analytical expression gives an empty-mold capacitance of 0.8257 pF, while the numerical simulations predict a value of 0.887 pF. The close agreement of these two values suggests that the numerical simulations take into account the secondary edge effects described previously. The material properties of the water–glycerin solution were measured using a simple dielectric cell and are in good agreement with values taken from the data sheet provided by the manufacturer. The dielectric constant of the solution was  $\varepsilon_{2*} \approx 46$ . This value was used in the analytical expression as well as the Maxwell simulations. When the mold is filled with water–glycerin solution, the analytical capacitance is 1.532 pF, while numerical simulations predict a value of 1.500 pF.

### Experimental Capacitance and Phase Data

Terminal admittance values were acquired using the dielectric sensor array system. Gain and phase were measured by the sensors and converted to capacitance and conductance values. Cross-talk between parallel-plate sensors was observed during experiments. The effect of the cross-talk on the measured capacitance was negligible considering that measured capacitance values from one sensor, driven alone and driven simultaneously with two other sensors, differed by less than 1%.

Figure 11 shows experimental results for an experiment at 90 kPa. The data exhibits a gradual increase in capacitance as the fluid flows through the mold. This gradual increase is predicted by numerical simulations and is due to edge effects of the parallel-plate setup. The water–glycerin solution is detected by the sensors before the liquid is actually between the plates. Numerical simulations can quantify this effect so that it can be factored out.

The signal-to-noise ratio (SNR) for the capacitance data is found by taking the magnitude of the signal and dividing it by the magnitude of the observed noise in the data set. Using channel 1 from Figure 11 as an example, the SNR is given by

$$\text{SNR}_{\text{cap}} = \frac{\text{signal}}{\text{noise}} = \frac{(2.31 - 1.67)}{0.01} = 64 \quad (20)$$

Converting to decibels yields an SNR of 18 dB. The uncertainty in the flow-front measurement can be found since the SNR of the flow-front measurement will be the same. The uncertainty calculation in the flow measurement is given by

$$\text{noise}_{\text{flow}} = \frac{\text{signal}}{\text{SNR}_{\text{cap}}} = \frac{(6.5)}{64} = 0.101 \quad (21)$$

thus, the uncertainty in the flow measurement is  $\pm 0.101$  in. or  $\pm 2.57$  mm.

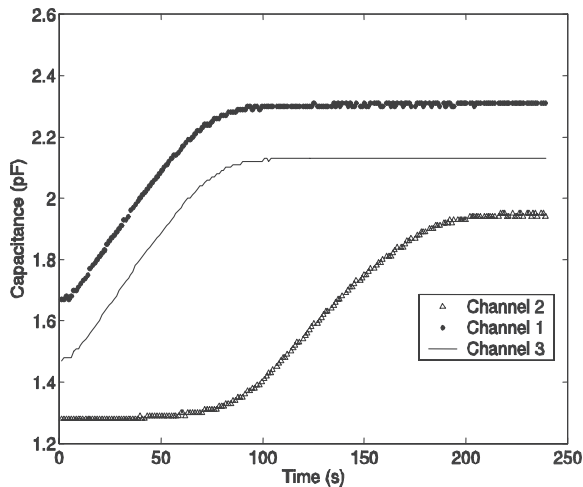


**Figure 11.** Capacitance as a function of time for three sensors at 90 kPa.

### Data Analysis

A mapping algorithm was developed to convert measured capacitance values to flow-front position as a function of time for each sensor. Figure 12 shows a graphical representation of this algorithm.

The algorithm includes a normalization procedure and curve-fitting routine detailed below:

- (1) Normalize experimental and numerical data. For this normalization procedure, assume only errors of the form  $ax + b$ . Normalize the data by subtracting the lowest value ( $b$ ) from each data point. Then divide each new data point by the highest value data point, eliminating  $a$ . This step is implemented in quadrants 1 and 2 of Figure 12.
- (2) Use a spline curve-fitting method to fit a curve to the normalized numerical data. A spline fit will draw curves between consecutive data points and will find the equation for each curve. Thus, there is an equation describing any region on the graph containing two consecutive points, instead of one equation describing the region encapsulated by all points. This step is implemented in quadrant 2.
- (3) Substitute in each experimental capacitance value (with its corresponding time) to this equation and find the distance at which this capacitance was measured. This step is implemented in quadrant 3.
- (4) Plot distance as a function of time for each sensor. This step is implemented in quadrant 4.

This method is used because it can easily be developed into a fast real-time algorithm once the respective look-up tables are generated for each sensor. For example, if the sensor

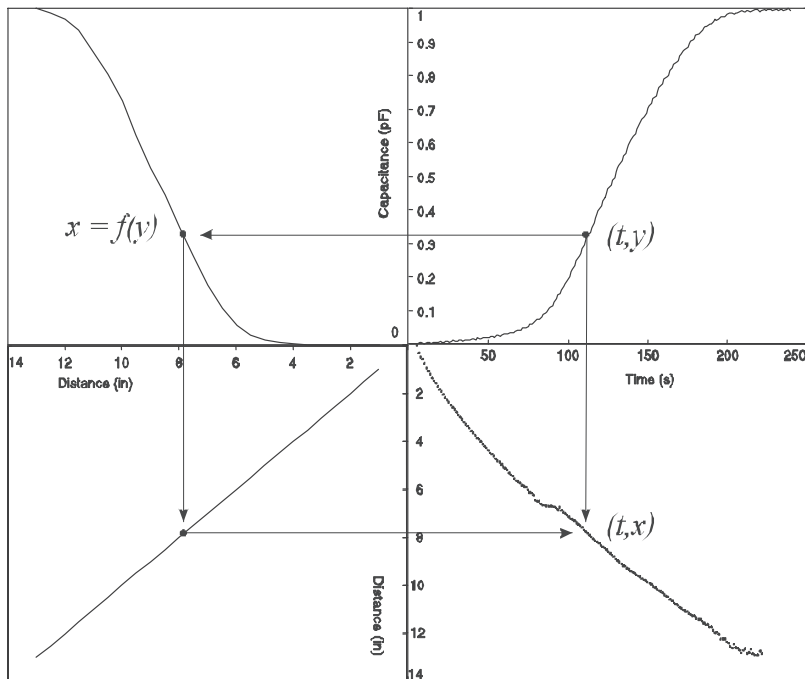


**Figure 12.** Graphical representation of the mapping algorithm used in the data analysis.

geometry and relative position on the mold is kept constant, only one numerical simulation is needed to correlate a measured capacitance with a distance along the mold. The graphical representation allows the reader to visualize the steps described above. The first and second quadrants of Figure 12 correspond to steps 1 and 2 of the algorithm above. Quadrant 3 corresponds to step 3 of the algorithm and quadrant 4 corresponds to step 4 of the algorithm. It should be noted that when the sensor geometry or position on the mold changes, additional numerical simulations will be needed in order to develop a mapping routine.

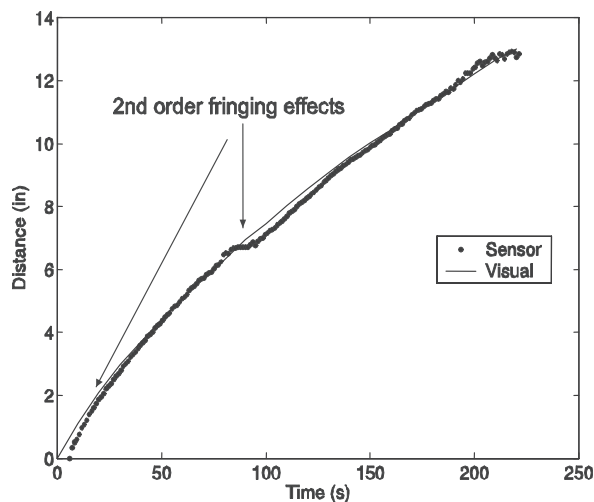
### Flow-front Position

Figure 13 shows that the fill-front measurement by the sensor system is in good agreement with the positions recorded by the video camera. The maximum difference between the visual and experimental data is approximately 0.2 in. (5 mm). The measurement accuracy is lowest in the region between the two sensors. This larger error in the region between the sensors is observed because the measurements are inherently less accurate due to fringing field effects.

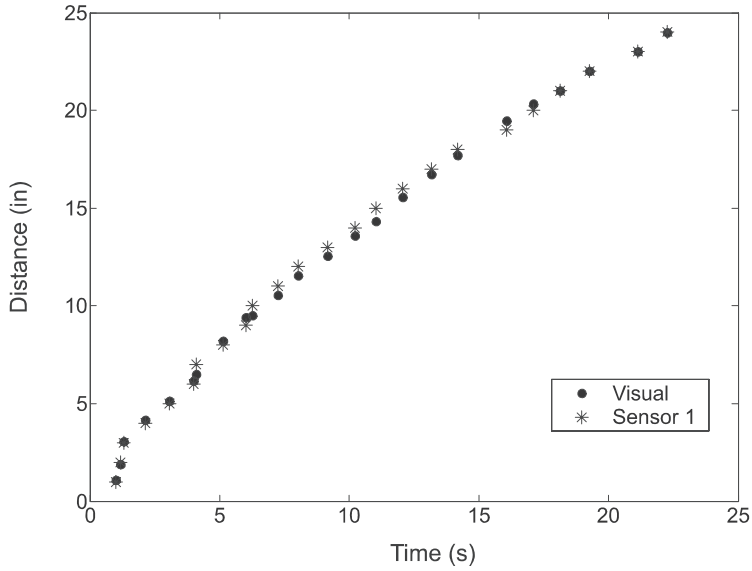
Although dielectric properties of resins are different from dielectric properties of glycerin–water mixtures, the measurement of fill-front position works equally well, because the sensor response is strong in both cases.

Figure 14 shows the visual and sensor data for fill-front position in a VARTM process using STYPOL 040-3676, a general purpose polyester resin. For this experiment, fringing field sensors, which require only one-sided access to the mold, were used. A good agreement between visual and sensor flow-front is observed.

After the filling process is complete, the sensor array switches into cure mode by measuring the curing process of the resin. An extended analysis of cure monitoring is the subject of a subsequent publication. As an illustration of dielectric spectroscopy signature, Figure 15 shows electrical parameter measurements as a function of frequency, for the resin during the curing phase.



**Figure 13.** Visual and experimental comparison of measured fill-front position at the centerline at 90 kPa.



**Figure 14.** Visual and experimental comparison of measured fill-front position at the centerline at 90 kPa for VARTM process using resin.

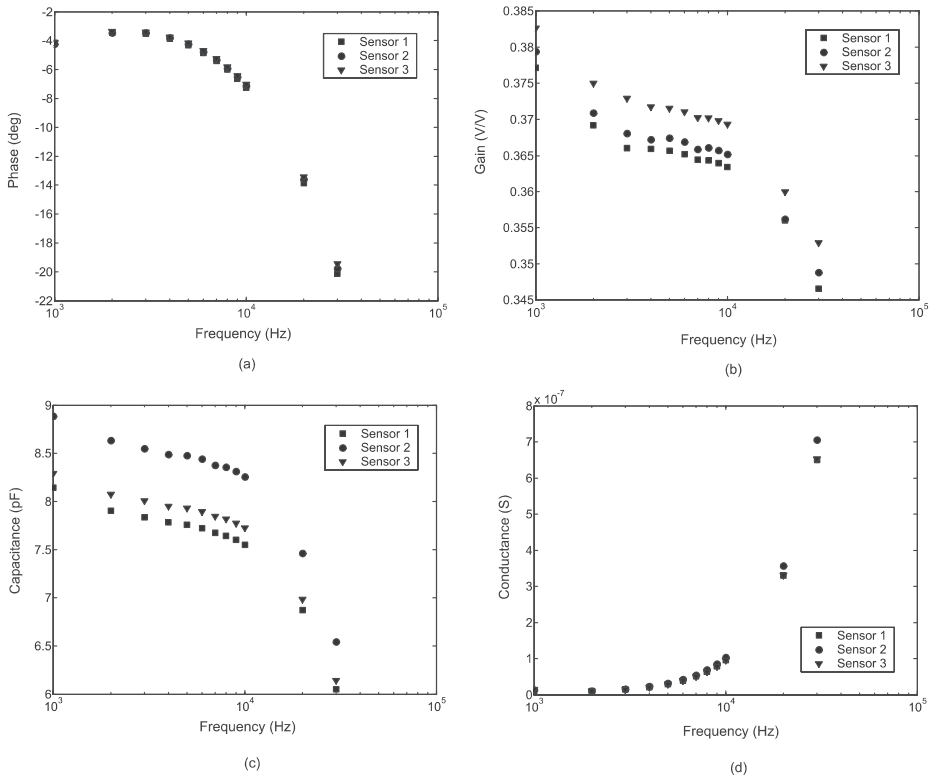


**Figure 15.** Electrical parameter measurements of the resin during cure, as a function of frequency: (a) phase, (b) gain, (c) capacitance, and (d) conductance.

Gain and capacitance show a similar monotonic decrease with frequency across all three channels, while phase and conductance monotonically increases with frequency. These spectroscopy measurements can be used as part of a calibration-based sensing technique to characterize the curing cycle of the resin.

## CONCLUSIONS AND FUTURE WORK

A distributed dielectric sensor array for measurement of flow-front location in RTM and VARTM processes was designed and tested with water–glycerin mixtures and with industrial resins. These sensors are also capable of monitoring the degree of cure of the resin. The developed technique allows for continuous sensing over the entire mold, while being completely noninvasive and not requiring embedded materials. The technique is useful for manufacturing of composite materials, where adaptive feed-forward control of the manufacturing process is desired. In addition, the sensor arrays can be made completely transparent, allowing for good visual calibration and the possibility of a coupled infrared sensor system.

Future work will focus on enhancing the resolution of this technique. It will involve modifying the existing circuitry to allow for more inputs and fabricating smaller transparent sensors. In addition, it will be necessary to measure flow-front position when the process utilizes multiple injection ports. The possibility of coupling the transparent sensors with a thermal or infrared sensor for temperature measurements will also be explored.

## ACKNOWLEDGMENTS

This project is supported by the Air Force Office of Scientific Research grant #F49620-02-1-0370, and National Science Foundation CAREER award #0093716.

The authors would like to thank graduate students Xiaobei Li and Kishore Sundara-Rajan, as well as undergraduate students Alexei Zyuzin and Gio Hwang for valuable discussions and assistance with experiments. Additionally, we would like to thank Mr. Walter Beauchamp from Boeing for providing useful comments and advice.

## REFERENCES

1. Han, K. and Lee, L.J. (1996). Dry Spot Formation and Changes in Liquid Composites Molding: I-Experiments, *Journal of Composite Materials*, **30**: 1458–1474.
2. Han, K., Lee, L.J. and Nakamura, S. (1996). Dry Spot Formation and Changes in Liquid Composites Molding: II-Modeling and Simulation, *Journal of Composite Materials*, **30**: 1475–1493.
3. Mogavero, J., Sun, J.Q. and Advani, S.G. (June 1997). A Nonlinear Control Method for Resin Transfer Molding, *Polymer Composites*, **18**(3): 412–417.
4. Yoon, M.K. and Sun, J.Q. (Jan. 2002). Adaptive Control of Flow Progression in Resin Transfer Molding, *Journal of Materials Processing & Manufacturing Science*, **10**(3): 171–182.
5. Shepard, D.D. (Nov. 1998). Resin Flow Front Monitoring Saves Money and Improves Quality, *SAMPE Journal*, **34**(6): 31–35.

6. Berker, B., Barooah, P. and Sun, J.Q. (Oct. 1997). Sequential Logic Control of Liquid Injection Molding with Automatic Vents and Vent-to-Gate Converters, *Journal of Materials Processing & Manufacturing Science*, **6**(2): 81–103.
7. Demirci, H.H. and Coulter, J.P. (Feb. 1996). A Comparative Study of Nonlinear Optimization and Taguchi Methods Applied to the Intelligent Control of Manufacturing Processes, *Journal of Intelligent Manufacturing*, **7**(1): 23–38.
8. Parthasarathy, S., Mantell, S.C., Stelson, K.A., Bickerton, S. and Advani, S.G. (1998). Real-Time Sensing and Control of Resin Flow in Liquid Injection Molding Processes, In: *Proceedings of the 1998 American Control Conference*, Vol. 4, pp. 2181–2184.
9. Ahn, S.H., Lee, W.I. and Springer, G.S. (1995). Measurement of the 3-Dimensional Permeability of Fiber Preforms using Embedded Fiber Optic Sensors, *Journal of Composite Materials*, **29**(6): 714–733.
10. Bernstein, J.R. and Wagner, J.W. (May 1997). Fiber Optic Sensors for use in Monitoring Flow Front in Vacuum Resin Transfer Molding Processes, *Review of Scientific Instruments*, **68**(5): 2156–2157.
11. Crosby, P.A., Powell, G.R., Fernando, G.F., Waters, D.N., France, C.M. and Spooncer, R.C. (1997). A Comparative Study of Optical Fibre Cure Monitoring Methods, In: *SPIE*, pp. 141–153.
12. Shepard, D.D. and Smith, K.R. (1999). Ultrasonic Cure Monitoring of Advanced Composites, *Sensor Review*, **19**(3): 187–191.
13. Fomitchov, P.A., Kim, Y.K., Kromine, A.K. and Krishnaswamy, S. (2002). Laser Ultrasonic Array System for Real-Time Cure Monitoring of Polymer-Matrix Composites, *Journal of Composite Materials*, **36**(15): 1889–1901.
14. Woerdeman, D.L. and Parnas, R.S. (Oct. 1995). Cure Monitoring in RTM using Fluorescence, *Plastics Engineering*, **51**(10): 25–&.
15. Tavakoli, S.M., Avella, M. and Phillips, M.G. (1990). Fiber Resin Compatibility in Glass Phenolic Laminating Systems, *Composites Science and Technology*, **39**(2): 127–145.
16. Barooah, P., Berker, B. and Sun, J.Q. (Jan. 1998). Lineal Sensors for Liquid Injection Molding of Advanced Composite Materials, *Journal of Materials Processing & Manufacturing Science*, **6**(3): 169–184.
17. Lee, C.W., Rice, B.P., Buczek, M. and Mason, D. (Nov. 1998). Resin Transfer Process Monitoring and Control, *SAMPE Journal*, **34**(6): 48–55.
18. Schwab, S.D., Levy, R.L. and Glover, G.G. (Apr. 1996). Sensor System for Monitoring Impregnation and Cure During Resin Transfer Molding, *Polymer Composites*, **17**(2): 312–316.
19. Alig, I., Jenninger, W., Junker, M. and deGraaf, L.A. (1996). Dielectric Relaxation Spectroscopy During Isothermal Curing of Semi-Interpenetrating Polymer Networks, *Journal of Macromolecular Science-Physics*, **B35**(3–4): 563–577.
20. Potapov, A.A. (Sept. 1993). Temperature-Dielectric Spectroscopy of Solutions, *Instruments and Experimental Techniques*, **36**(5): 772–776.
21. Kranbuehl, D., Hood, D., Kriss, A., Barksdale, R., Loos, A.C., Macrae, J.D. and Hasko, G. (Mar. 1996). In situ FDEMS Sensing and Modeling of Epoxy Infiltration, Viscosity and Degree of Cure During Resin Transfer Molding of a Textile Preform, *Abstracts of Papers of the American Chemical Society*, **211**: 17–MSE.
22. Kranbuehl, D., Hoff, M., Eichinger, D., Clark, R. and Loos, A. (1989). Monitoring and Modeling the Cure Processing Properties of Resin Transfer Molding Resins, *International SAMPE Symposium and Exhibition*, **34**: 416–425.
23. Kranbuehl, D.E., Kingsley, P., Hart, S., Hasko, G., Dexter, B. and Loos, A.C. (Aug. 1994). In-Situ Sensor Monitoring and Intelligent Control of the Resin Transfer Molding Process, *Polymer Composites*, **15**(4): 299–305.
24. Kranbuehl, D., Delos, S., Hoff, M., Weller, L., Haverty, P. and Seeley, J. (1988). Frequency-Dependent Dielectric Analysis – Monitoring the Chemistry and Rheology of Thermosets During Cure, *ACS Symposium Series*, **367**: 100–112.

25. Rooney, M., Biermann, P.J., Carkhuff, B.G., Shires, D.R. and Mohan, R.V. (1998). Development of In-Process RTM Sensors for Thick Composite Sections, In: *Proceedings of the 1998 American Control Conference*, Vol. 6, pp. 3875–3878.
26. Skordos, A.A., Karkanis, P.I. and Partridge, I.K. (Jan. 2000). A Dielectric Sensor for Measuring Flow in Resin Transfer Moulding, *Measurement Science & Technology*, **11**(1): 25–31.
27. von Hippel, A. (1995). *Dielectric Materials and Applications*, Artech House, Boston, MA.
28. Matis, I.G. (1966). Method and Equipment for Determining the Dielectric Constant of Polymer Materials with One-sided Access, *Polymer Mechanics*, **2**(4): 380–383.
29. Senturia, S.D., Sheppard, N.F., Poh, S.Y. and Appelman, H.R. (Feb. 1981). The Feasibility of Electrical Monitoring of Resin Cure with the Charge-Flow Transistor, *Polymer Engineering and Science*, **21**(2): 113–118.
30. Senturia, S.D., Sheppard Jr., N.F., Lee, H.L. and Day, D.R. (1982). In-Situ Measurement of the Properties of Curing Systems With Microdielectrometry, *Journal of Adhesion*, **15**(69): 69–90.
31. Senturia, S.D. and Garverick, S.L. (Dec. 1983). Method and Apparatus for Microdielectrometry, US Patent No.4,423,371.
32. Zaretsky, M.C., Mouayad, L. and Melcher, J.R. (Dec. 1988). Continuum Properties from Interdigital Electrode Dielectrometry, *IEEE Transactions on Electrical Insulation*, **23**(6): 897–917.
33. Washabaugh, A., Schlicker, D.E., Mamishev, A.V., Zahn, M. and Goldfine, N. (1999). Dielectric Sensor Arrays for Monitoring of Aging in Composites and Other Low-Conductivity Media, In: *SPIE Conference*.
34. Mijovic, J. and Sy, J.W. (Dec. 2000). Dipole Dynamics and Macroscopic Alignment in Molecular and Polymeric Liquid Crystals by Broad-Band Dielectric Relaxation Spectroscopy, *Macromolecules*, **33**(26): 9620–9629.
35. Kranbuehl, D.E., Delos, S.E. and Yi, E. (1985). Measurement and Application of Dielectric Properties, *SPIE Technical Papers*, **31**(311): 73–90.
36. Mamishev, A.V., Du, Y., Lesieutre, B.C. and Zahn, M. (Apr. 1999). Development and Applications of Fringing Electric Field Dielectrometry Sensors and Parameter Estimation Algorithms, *Journal of Electrostatics*, **46**(2–3): 109–123.
37. Goldfine, N.J. (Mar. 1993). Magnetometers for Improved Materials Characterization in Aerospace Applications, *Materials Evaluation*, **51**(3): 396–405.
38. Mamishev, A.V., Lesieutre, B.C. and Zahn, M. (1998). Optimization of Multi-Wavelength Interdigital Dielectrometry Instrumentation and Algorithms, *IEEE Transactions on Dielectrics and Electrical Insulation*, pp. 408–420.
39. Ebersold, C.B. (2000). Racetracking and Porous Medium Displacement in Resin Transfer Molding, Department of Mechanical Engineering, University of Washington.

